Coupling of elasticity to capillarity in soft aerated materials

Lucie Ducloué, Olivier Pitois, Julie Goyon, Xavier Chateau, Guillaume Ovarlez

Soft Matter

PAPER

Coupling of elasticity to capillarity in soft aerated materials

Cite this: *Soft Matter*, 2014, **10**, 5093

Lucie Ducloué,* Olivier Pitois, Julie Goyon, Xavier Chateau and Guillaume Ovarlez

Received 24th January 2014
Accepted 28th April 2014

DOI: 10.1039/c4sm00200h

www.rsc.org/softmatter

We study the elastic properties of soft solids containing air bubbles. Contrary to standard porous materials, the softness of the matrix allows for a coupling of the matrix elasticity to surface tension forces acting on the bubble surface. Thanks to appropriate experiments on model systems, we demonstrate how the elastic response of the soft porous solid is governed by two dimensionless parameters: the gas volume fraction and a capillary number comparing the elasticity of the matrix with the stiffness of the bubbles. Furthermore, we show that our experimental results are accurately predicted by computations of the shear modulus through a micro-mechanical approach.

1 Introduction

Complex systems of a dispersed phase in a solid matrix can behave very differently from one of their components taken alone. Their broad range of properties explains that examples of dispersions such as composites[1] or porous media[2] are widespread in the industry. In all dispersions, interfacial forces can appear at the boundary between the dispersed phase and the continuous matrix. A coupling of surface tension forces to the bulk elasticity of a solid has been evidenced in soft systems like biological tissues,[3] or through the deformation of soft substrates like polymers at the contact line with a drop resting on the solid,[4] which has been modeled by recent theoretical and numerical work on elasto-capillary phenomena.[5] Understanding the coupling of bubble mechanics to the matrix elasticity is also essential for cavitation rheology techniques[6,7] and for the stability of bubbles in complex fluids.[8,9] Capillary forces also affect the overall mechanical properties of nanoporous media.[10] For larger pores, because of the hardness of the matrix in usual porous media, the influence of interfacial effects on the overall properties of the saturated material is negligible.[11] Dispersions in softer materials could allow for observable coupling of interfacial forces to the bulk elasticity of the solid at larger scales than the nanometer. Many dense suspensions[12] of geological interest, like muds, or with industrial applications, like fresh concrete or emulsions, behave as soft elastic solids below a critical level of stress.[13] To study the role of surface tension forces in soft elastic materials, we investigate the elastic behaviour of dispersions of bubbles in concentrated emulsions. Those aerated emulsions, which have applications in the food[14] and cosmetic[15] industries, have been the subject of rheological and stability studies.[16–18] However, their overall elastic properties have not yet been studied in detail.

In dispersions of bubbles in a soft material, coupling between the elasticity of the matrix and capillary effects is expected to occur through bubble deformation. The elastic deformation of the matrix tends to deform the bubbles and surface tension forces will thus act to minimize the area of the bubble by maintaining a spherical shape. The limit case of negligible surface tension forces is a soft porous medium. Theoretical work shows that adding holes in a solid softens it.[11] In the limit case of predominant surface tension forces compared to the matrix elasticity, a bubble should no longer be deformable and should behave as a rigid inclusion with no shear stiffness. Experimental and theoretical studies have shown that rigid beads in a soft solid strengthen the solid.[19] The case of rigid bubbles is similar except for the boundary conditions, changed from no-slip for beads to full-slip for bubbles. Theoretical models in the dilute limit predict a strengthening of the dispersion when adding rigid bubbles.[11] Between those two limit cases, more work is needed to investigate the elastic response of the soft aerated solid. In this work, we restrain to the range of gas volume fraction $\phi < 50\%$, so that we do not consider foams of those materials, in which the bubbles are deformed by geometrical constraints. We design model systems and appropriate experimental methods that allow us to measure the shear modulus of dispersions of monodisperse bubbles embedded in a medium of chosen elasticity. We then extract the key parameters governing the overall elastic response of the systems, and compare our experimental results to estimates of the elastic modulus through a micro-mechanical approach.

2 Experimental aspects

The dispersion matrices we choose are concentrated oil in water emulsions of shear moduli ranging from 100 to 1000 Pa. Concentrated emulsions behave as soft elastic solids for

Laboratoire Navier (UMR CNRS 8205), Université Paris-Est, 77420 Champs-sur-Marne, France. E-mail: lucie.ducloue@ifsttar.fr

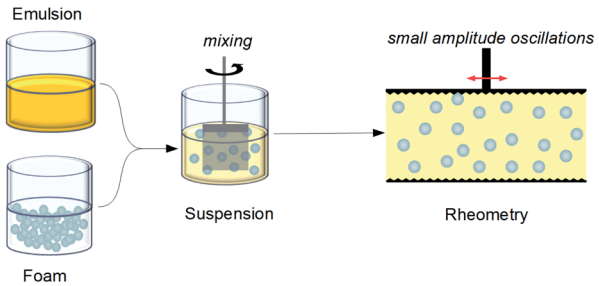

Fig. 1 Schematic of the experimental protocol (bubbles not to scale). A concentrated emulsion is mixed with a monodisperse foam to obtain a dispersion of monodisperse bubbles in a yield stress fluid. The elastic modulus of the dispersion is then measured by applying small amplitude oscillations.

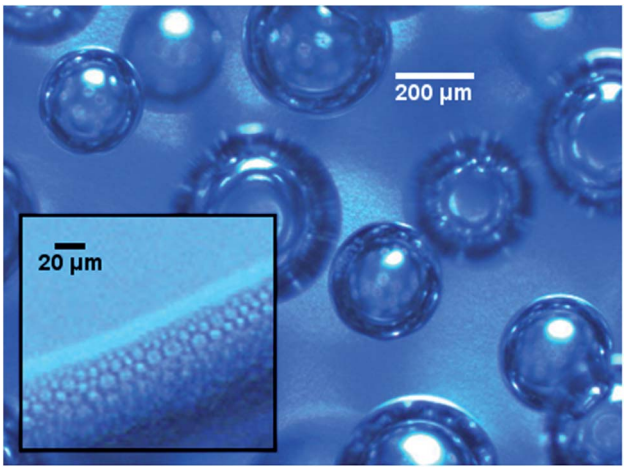

Fig. 2 Microphotograph of a dispersion of monodisperse bubbles ($R = 200$ μm) in emulsion (2). The image is taken in the bulk of a sample of the material deposited on a glass slide. The emulsion is transparent, allowing for the visualisation of in-depth bubbles that thus do not have the same apparent radius. Inset: close-up of droplets of emulsion (2) at the interface with a bubble on the surface of the glass.

stresses well below their yield stress.[20] The emulsions were produced with a patented Couette emulsifier.[21,22] Unless otherwise indicated, the radius of the droplets measured by laser granulometry is around 1 to 2 μm (the polydispersity is around 20%), which, at the considered gas volume fractions, should ensure that there is scale separation between the drops and the bubbles, and consequently validate the use of the emulsion as an elastic continuous medium embedding the bubbles.[23] In all the systems, the yield stress of the emulsion is high enough to ensure that no bubble rise occurs at rest or during measurements.[24] Most dispersions are prepared by gently mixing the emulsion with a separately produced monodisperse foam. A schematic of the experimental protocol is presented in Fig. 1. The foams are obtained by blowing nitrogen plus a small amount of perfluorohexane (C_6F_{14}) through a porous glass frit or through needles; we are able to produce nearly monodisperse foams with average bubble radii R_b ranging from 40 μm to 800 μm. The bubble size is measured by image analysis on a foam sample squeezed between two glass slides separated by spacers of known thickness. Coarsening is strongly reduced by the presence of C_6F_{14},[25] meaning that the bubble size is stable during measurements. The continuous phase of the foam is the same as the one in the emulsion, ensuring that mixing is easy and does not induce any chemical effect on the dispersions. The mixing with the foam adds a small amount of continuous phase to the emulsion. To ensure that, for a series of experiments at different gas volume fractions in a given emulsion, the elastic modulus of the matrix in the dispersions remains the same, we added controlled amounts of pure continuous phase in order to reach the same oil volume fraction in the emulsion.[17,18] An example of a dispersion of bubbles in an emulsion is shown in Fig. 2. The composition of all the tested emulsions is indicated in Table 1, and illustrates the variety of chemical compositions, surface tensions and elastic properties of the matrix that were used to perform the study. Surface tension measurements have been performed with a Teclis Tracker tensiometer, using either a pendant drop or a rising bubble method. All the experiments are performed at 25 °C.

The shear modulus of the dispersions is measured using a control stress rheometer by imposing small amplitude oscillations at a frequency of typically 1 Hz. The oscillatory stress is chosen to be well below the yield stress of the systems, so that the oscillations are performed in the linear elastic regime of each material. At this frequency, the loss modulus of the systems is negligible. The geometry used to perform the rheometrical measurements is chosen according to the bubble size: for $R_b \leq 50$ μm, the material is sheared between parallel plates (radius $R = 25$ mm; gap $h = 2.5$ mm). The planes are serrated to prevent slippage of the dispersion.[12] Dispersions containing bigger bubbles require a larger thickness of the sheared

Table 1 Synthetic description of all the emulsions used as matrices in the bubble dispersions: nature and volume fraction of the oil dispersed phase, composition of the aqueous continuous phase (including the surfactant) and relevant physical constants for the determination of the capillary number: elastic modulus of the matrix, and surface tension between air and the continuous phase. The composition given is the one of the matrices actually embedding the bubbles

	Oil – vol fraction	Continuous phase	$G'(0)$ (Pa)	γ (mN m^{-1})
Emulsion (1a)	Silicon (V20, Chimie Plus) – 75%	Forafac® (Dupont™) 4 wt% in water	230	15.5 ± 0.1
Emulsion (1b)	Silicon (V20, Chimie Plus) – 73%	Forafac® (Dupont™) 4 wt% in water	163	15.5 ± 0.1
Emulsion (2)	Silicon (V350, Chimie Plus) – 79%	TTAB (Alpha–Aesar) 3 wt% in water/glycerol 50/50 w/w	650	35.5 ± 0.1
Emulsion (3)	Dodecane (Acros organics) – 73%	SDS (Sigma) 2.7 wt% in water	285	36 ± 1
Emulsion (4)	Silicon (V350, Chimie Plus) – 70%	TTAB (Alpha–Aesar) 3 wt% in water/glycerol 36/64 w/w	799	35 ± 1

material and are studied in Couette-like devices: for 50 μm < R_b < 800 μm, we use a vane in cup (exceptionally a serrated bob in cup) geometry (inner radius R_i = 12.5 mm; outer radius R_o = 18 mm), and for $R_b \geq 800$ μm, we use vane in cup geometries (either R_i = 12.5 mm and R_o = 25 mm or R_i = 22.5 mm and R_o = 45 mm).

3 Results

3.1 Control parameters

We first investigate the influence of the experimental parameters that can easily be tuned in our systems. We start by studying the dependence of the elasticity on the bubble radius R_b by preparing dispersions of various bubble radii in the same emulsion. In a first series of experiments, we add bubbles of R_b = (50 ± 10) μm (10 μm being the width of the volume-weighed bubble radius distribution) at various gas volume fractions ϕ in emulsion (3) (see Table 1 for details). Those bubbles are slightly more polydisperse than is generally used for this study, because of the foam production technique. The shear modulus $G'(\phi)$ of the dispersions is measured to be slightly decreasing with ϕ. This result is reported in dimensionless quantities $\hat{G}(\phi) = G'(\phi)/G'(0)$ as a function of ϕ as shown in Fig. 3. We then prepare dispersions of larger bubbles in emulsion (3): a series with R_b = (143 ± 17) μm and another one with R_b = (800 ± 40) μm. The results for $\hat{G}(\phi)$ are also shown in Fig. 3. The measurements show that the larger the bubbles, the softer the dispersion. This result can be understood as a manifestation of a simple physical effect, as has already been evidenced in ref. 18 (see also ref. 26 and 27 for the effect of bubble deformation on the viscosity of bubbly Newtonian fluids), that the interfacial energy to volume ratio is lower in larger bubbles, resulting in least bubble resistance to deformation.

We keep the bubble size constant, and vary the elastic modulus of the matrix; we prepare dispersions of R_b = 143 μm bubbles in emulsion (3) and of R_b = (150 ± 10) μm bubbles in emulsion (4) (see Table 1). In the two series of experiments, the bubble sizes are close and the surface tension is similar, but $G'(0)$ is almost three times higher in emulsion (4). $\hat{G}(\phi)$ is plotted for both systems in the inset shown in Fig. 3. As observed on the previous suspensions, $\hat{G}(\phi)$ is a decreasing function of ϕ, and this decrease is all the stronger as $G'(0)$ is high. To quantify the competition between the matrix elasticity and the bubble resistance to deformation, we introduced a capillary number,

$$Ca = \frac{G'(0)}{2\gamma/R_b} \quad (1)$$

which compares the shear modulus of the dispersion medium and the interfacial stress scale which is the capillary pressure in the bubbles. This dimensionless number scales as the reciprocal of the elasto-capillary number and has been defined for instance in ref. 5 for a similar geometry and derived from an energetic argument.

The use of our model experimental systems allows us to vary independently the three physical parameters that influence *Ca*. To quantify the relevance of *Ca* on the overall elastic response of the dispersion at a given ϕ, we can thus perform two series of experiments with close R_b, but with a very different capillary pressure because of a very different surface tension, and we adjust the elastic modulus in one of the emulsions so that *Ca* is similar in both systems. The two experimental systems are as follow: the first one is dispersions of R_b = 143 μm of radius bubbles in emulsion (3), which leads to *Ca* = 0.57 ± 0.08, and the second one is dispersions of (129 ± 10) μm of radius bubbles in emulsion (1b) for which *Ca* = 0.70 ± 0.08. We

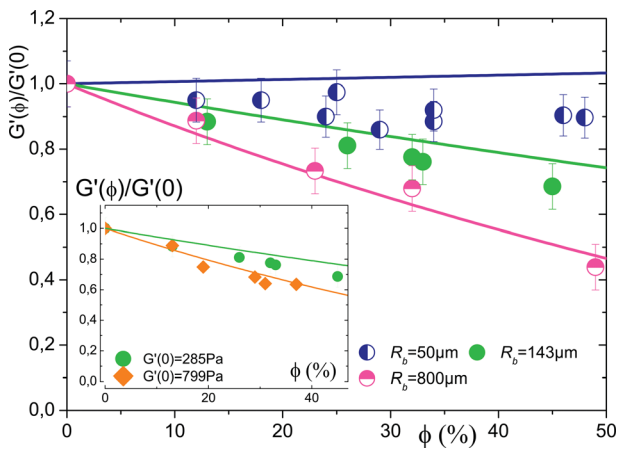

Fig. 3 Dimensionless elastic modulus $\hat{G}$ as a function of the gas volume fraction ϕ for dispersions with three different bubble radii R_b in emulsion (3) [see legend]. The full lines are the computed $\hat{G}_{homog}(\phi)$ for *Ca* = 0.23 (dark blue), *Ca* = 0.57 (green) and *Ca* = 3.2 (pink); experimentally measured *Ca*: 0.23 ± 0.05, 0.57 ± 0.08, 3.2 ± 0.4. Inset: $\hat{G}$ as a function of ϕ for dispersions of $R_b \approx 150$ μm in ● emulsion (3) and ♦ emulsion (4). The full lines are the computed $\hat{G}_{homog}(\phi)$ for *Ca* = 0.57 (green) and *Ca* = 1.65 (orange); experimentally measured *Ca*: 0.57 ± 0.08 and 1.65 ± 0.15.

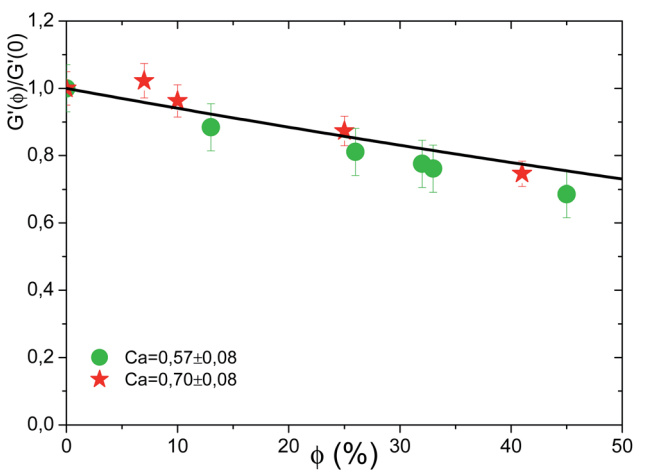

Fig. 4 Effect of a change in the surface tension: dimensionless elastic modulus $\hat{G}$ as a function of ϕ for dispersions of ● R_b = 143 μm bubbles in emulsion (3) and ★ R_b = 129 μm bubbles in emulsion (1b). The surface tension is much lower in emulsion (1b), but $G'(0)$ has been chosen to get close values for *Ca* in both systems. The experimentally measured *Ca* are 0.57 ± 0.08 and 0.70 ± 0.08. The full line is the computed $\hat{G}_{homog}(\phi, Ca)$ at *Ca* = 0.63, which is compatible with both systems, given the experimental precision on the value of *Ca*.

observed that the measured values of $\hat{G}(\phi, Ca)$ are very close, as can be seen in Fig. 4. The value of Ca unequivocally determines the elastic behaviour of the dispersion at a given ϕ.

3.2 Limit cases for *Ca*

We now investigate the limit value of $Ca \to \infty$, for which surface tension forces are negligible and the bubbles can be assimilated to voids in the matrix. This is the case in usual porous materials. We design a system in which surface tension effects are bound to be poor; we indeed include the biggest bubbles of this study, of radius (1 ± 0.1) mm, in emulsion (2), which has a high elastic modulus (see Table 1). Note that for this system the bubbles are injected directly in the emulsion in a tee-junction in a milli-fluidic device. As before, we measure the elastic modulus of the dispersion at various ϕ. The experimental data points for the dimensionless modulus $\hat{G}(\phi)$ are shown in Fig. 5, and compared to the dilute limit for dispersions of holes in an elastic medium, which can be analytically computed:[11] $\hat{G}(\phi, Ca \to \infty) = 1 - \frac{5}{3}\phi$. We observe that $\hat{G}$ is a decreasing function of ϕ, and that for a low gas volume fraction the measured $\hat{G}$ is close to the dilute limit. The exact value of Ca in this system is 9.0 ± 1.2 and this result shows that the theoretical dilute limit for spherical holes in an elastic medium is already a good estimate of $\hat{G}(\phi \to 0, Ca)$ at $Ca \sim 10$.

The limit case of $Ca \to 0$ also leads to simplification: the bubbles are stiff compared to the matrix and the dispersion is made of rigid spheres with a full slip boundary condition in an elastic medium. The theoretical dilute limit can be computed[11] as $\hat{G}(\phi, Ca = 0) = 1 + \phi$ and is shown in Fig. 5. An experimental validation of this limit with our systems may be biased, because increasing the capillary pressure would mean reducing R_b, and we might no longer assume scale separation between the bubbles and the oil droplets. As our experimental systems are not suited to perform experiments at small capillary numbers, more work would be needed to design suitable model materials to investigate this limit.

From $Ca \to 0$ to $Ca \to \infty$, $\hat{G}(\phi, Ca)$ turns from an increasing to a decreasing function of ϕ. Between these two extreme values, we have observed on the dispersion of the smallest bubbles in emulsion (3), as has already been shown in Fig. 3, that $G'(\phi)$ has little variation with ϕ and is comparable to $G'(0)$. The capillary number in this system is $Ca = 0.23 \pm 0.05$. To further check the peculiarity of this value of Ca, we prepare another dispersion of small bubbles $R_b = (41 \pm 5)$ μm in emulsion (1a) (see Table 1), with a close capillary number: $Ca = 0.30 \pm 0.05$. $\hat{G}(\phi, Ca)$ for both dispersions of small bubbles is shown in Fig. 5. We observe that in both systems, $\hat{G}(\phi, Ca)$ exhibits little dependence on the gas volume fraction, and is of order 1. The non-perturbative effect of bubble addition in the matrix can be seen as an experimental validation of previous micro-mechanical calculations[28,29] which have shown that a spherical bubble of radius R_b and surface tension γ in an elastic medium can be described as an equivalent elastic sphere of radius R_b and no surface tension. This has been shown to result mostly from the work of the capillary pressure when the bubble is deformed under a strain ε (ref. 28), leading to an increase of energy that scales as $\gamma\varepsilon^2$, which is analogous to an elastic energy. If the equivalent elasticity of the sphere is equal to that of the matrix, the bubbles are non-perturbative and $\hat{G}(\phi) = 1$.

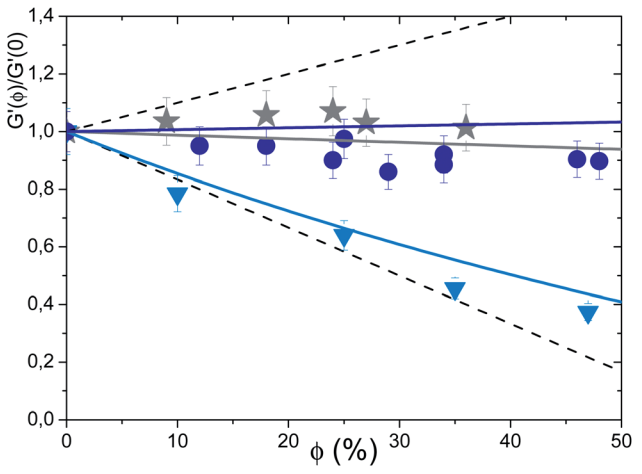

Fig. 5 Remarkable values of Ca: $Ca \to \infty$: $\hat{G}(\phi)$ for dispersions of ▼ R_b = 1 mm bubbles in emulsion (2). The full line is the computed $\hat{G}_{homog}(\phi, Ca)$ at $Ca = 9.0$ (light blue); experimentally measured Ca: 9.0 ± 1.2. $Ca \approx 0.25$: dimensionless elastic modulus $\hat{G}$ for dispersions of ● $R_b = 50$ μm bubbles in emulsion (3) and ★ $R_b = 41$ μm in emulsion (1a). The full lines are the computed $\hat{G}_{homog}(\phi, Ca)$ at $Ca = 0.23$ (dark blue) and $Ca = 0.30$ (grey); experimentally measured Ca: 0.23 ± 0.05, 0.30 ± 0.05. The dashed lines are the dilute limits for rigid (top) and fully deformable (bottom) spheres, with a full slip boundary condition.

3.3 Micro-mechanical approach

The equivalence of a bubble in an elastic medium and an elastic sphere in that medium can be quantified through a micro-mechanical approach; the equivalent elasticity of a bubble in a matrix $G'(0)$ can be written as a function of $G'(0)$ and Ca:[28,29]

$$G^{eq} = G'(0)\frac{8}{3 + 20Ca} \tag{2}$$

with Ca defined in eqn (1). The expression of G^{eq} shows that Ca introduced above does not actually compare the equivalent elasticity of the bubble with that of the matrix. This explains why the overall elasticity of the dispersion is unperturbed by the presence of the bubbles for a somewhat unnatural value of Ca around 0.2 to 0.3, which can be understood due to the computation of G^{eq}: $G^{eq} = G'(0)$ for $Ca = 1/4$. Relying on the equivalent elastic sphere model for a bubble, a micro-mechanical approach allows us to compute the overall elastic properties of the dispersions at finite Ca. The overall elasticity of a composite material made of elastic spheres in a matrix of another elastic material in the semi-dilute limit can be computed as a function of Ca and ϕ, in the framework of the Mori–Tanaka scheme:[28,29]

$$\hat{G}_{homog}(\phi, Ca) = 1 - \frac{\phi(4Ca - 1)}{1 + \frac{12}{5}Ca - \frac{2}{5}\phi(1 - 4Ca)} \tag{3}$$

Note that this expression is compatible with the previously discussed limits of $Ca \to \infty$, $Ca \to 0$ and $Ca = 1/4$. Predictions

of the model for $\hat{G}(\phi, Ca)$ at the experimentally measured Ca are plotted as full coloured lines shown in Fig. 3–5. A comparison of $\hat{G}_{\mathrm{homog}}(\phi, Ca)$ with $\hat{G}(\phi, Ca)$ for all the systems we used, at all tested gas volume fractions is presented in Fig. 6. Experimental measurements and computations are generally in good agreement all over the range of systems we investigated.

As we have seen that the two dimensionless parameters Ca and ϕ are enough to understand and predict the elasticity of the dispersions, we now plot $\hat{G}(\phi, Ca)$ as a function of Ca, for 4 values of ϕ, as shown in Fig. 7. As can be noticed from the graphs 3 to 5, the achieved values of ϕ are different for all tested systems. To be able to plot $\hat{G}(\phi, Ca)$ at a given ϕ, we interpolate the experimental data at the exact values of ϕ used for plotting as shown in Fig. 7. The full lines are computations of $\hat{G}_{\mathrm{homog}}(\phi, Ca)$. As expected, $\hat{G}(\phi, Ca)$ is a decreasing function of Ca; higher values of Ca correspond to more deformable bubbles that lower the overall elastic modulus of the dispersions. The non-perturbative effect of the bubbles for $Ca = 1/4$ is evidenced by the crossing of $\hat{G}_{\mathrm{homog}}(\phi, Ca)$ at 1 for $Ca = 0.25$, whatever the gas volume fraction. Below this value, the increase of $\hat{G}_{\mathrm{homog}}(\phi, Ca)$ is consistent with previously discussed theoretical limits, but could not be investigated with our experimental systems. The series of data points at $Ca = 0.23 \pm 0.05$ does not fit in the increasing $\hat{G}_{\mathrm{homog}}(\phi, Ca)$ regime, perhaps because of broader polydispersity; indeed, the uncertainty on the value of Ca mainly arises from the width of the bubble radius distribution and the value of Ca for the largest bubbles in this system is for instance higher than 0.25. A model computing $\hat{G}_{\mathrm{homog}}(\phi, Ca)$ as a function of the whole measured distribution of radii may better represent the experimental data and remains to be developed.

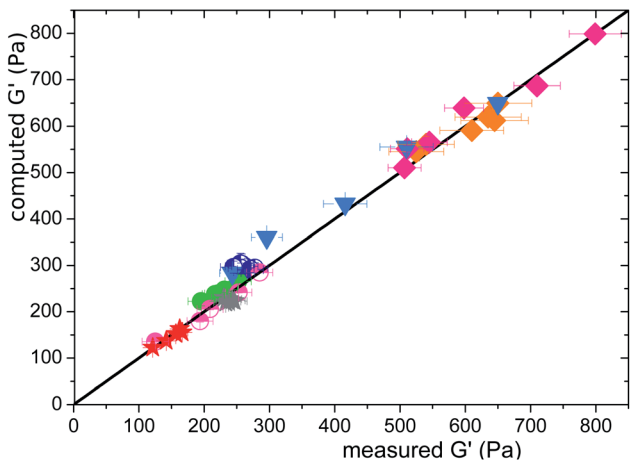

Fig. 6 Consistency between G' and G'_{homog} for all tested systems. ★: emulsion (1), ▼: emulsion (2), ●: emulsion (3), ◆: emulsion (4).

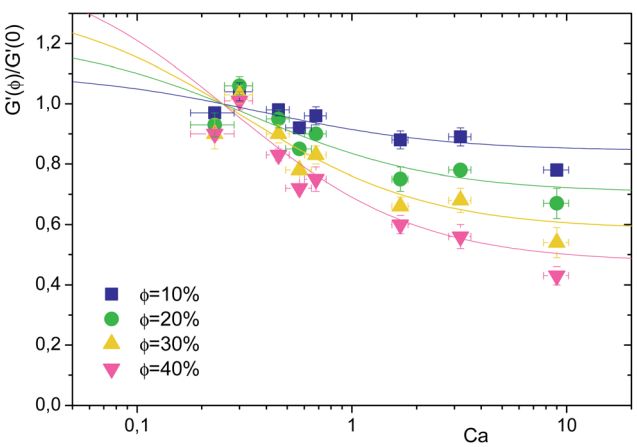

Fig. 7 Dimensionless elastic modulus $\hat{G}$ as a function of Ca for four different values of the gas volume fraction. The dots are interpolated experimental data points, the full lines are $\hat{G}_{\mathrm{homog}}(\phi, Ca)$.

4 Conclusions

This experimental study on model materials shows that the overall elasticity of dispersions of monodisperse bubbles in a soft elastic medium is governed by only two parameters: the gas volume fraction and a capillary number which compares the matrix elasticity with the bubble capillary stress. The generality of this result is experimentally demonstrated by the consistency of data on various systems, and is enhanced by the good agreement of the experimental data with micro-mechanical estimates of the shear modulus, even if the case $Ca < 1/4$ is still to be studied. A new model system remains to be designed to achieve this goal. Because the physical mechanisms evidenced by our work are not material-specific, the dependence of $\hat{G}$ on ϕ and Ca determined for macroscopic bubbles in model systems should still hold for a broader class of elastic materials containing air bubbles, for instance nanoporous media. Besides, the quantitative agreement between micro-mechanical estimates and measurements allows us to make predictions for the elastic modulus of a bubbly solid, and bubble addition could thus be a means of finely tuning material elasticity without modifying the composition of the matrix.

Understanding the coupling of many bubbles in an elastic medium could also give insights into the mechanical behaviour of soft solids like polymers undergoing multiple cavitation. Further refinements in the micro-mechanical computations, especially taking polydispersity into account, could allow for better representation of some of the data we presented, but also prove useful for the long time evolution of our systems; at longer time scales than investigated for the present study, bubble ripening is indeed expected to occur. This will probably affect the evolution of the shear modulus with time, and this evolution could perhaps be followed to derive the kinetics of bubble ripening.

Acknowledgements

Financial support from Saint-Gobain Recherche (Aubervilliers, France) is acknowledged.

References

1 F. L. Matthews and R. D. Rawlings, *Composite materials: engineering and science*, Woodhead Publishing, 1999.

2 O. Coussy, *Mechanics and physics of porous solids*, John Wiley & Sons, 2011.
3 J. A. Clements, R. F. Hustead, R. P. Johnson and I. Gribetz, *J. Appl. Physiol.*, 1961, **16**, 444–450.
4 R. Pericet-Cámara, A. Best, H.-J. Butt and E. Bonaccurso, *Langmuir*, 2008, **24**, 10565–10568.
5 D. L. Henann and K. Bertoldi, *Soft Matter*, 2014, **10**, 709–717.
6 J. Cui, C. H. Lee, A. Delbos, J. J. McManus and A. J. Crosby, *Soft Matter*, 2011, **7**, 7827–7831.
7 A. Delbos, J. Cui, S. Fakhouri and A. J. Crosby, *Soft Matter*, 2012, **8**, 8204–8208.
8 M. Fyrillas, W. Kloek, T. van Vliet and J. Mellema, *Langmuir*, 2000, **16**, 1014–1019.
9 W. Kloek, T. van Vliet and M. Meinders, *J. Colloid Interface Sci.*, 2001, **237**, 158–166.
10 H. Duan, J. Wang, Z. Huang and B. Karihaloo, *J. Mech. Phys. Solids*, 2005, **53**, 1574–1596.
11 L. Dormieux, D. Kondo and F.-J. Ulm, *Microporomechanics*, Wiley. com, 2006.
12 P. Coussot, *Rheometry of pastes, suspensions, and granular materials: applications in industry and environment*, Wiley, 2005.
13 P. Coussot, *Rhéophysique, SOFEDIS*, 2012.
14 G. A. van Aken, *Colloids Surf., A*, 2001, **190**, 333–354.
15 D. Balzer, *Tenside, Surfactants, Deterg.*, 1991, **28**, 419–427.
16 A. Salonen, R. Lhermerout, E. Rio, D. Langevin and A. Saint-Jalmes, *Soft Matter*, 2011, **8**, 699–706.
17 J. Goyon, F. Bertrand, O. Pitois and G. Ovarlez, *Phys. Rev. Lett.*, 2010, **104**, 128301.
18 M. Kogan, L. Ducloué, J. Goyon, X. Chateau, O. Pitois and G. Ovarlez, *Rheol. Acta*, 2013, 1–17.
19 F. Mahaut, X. Chateau, P. Coussot and G. Ovarlez, *J. Rheol.*, 2008, **52**, 287.
20 T. Mason, J. Bibette and D. Weitz, *Phys. Rev. Lett.*, 1995, **75**, 2051.
21 J. M. J. Bibette and T. Mason, Emulsion Manufacturing Process, *EP Pat.*, 0,843,589, 2004.
22 T. Mason and J. Bibette, *Langmuir*, 1997, **13**, 4600–4613.
23 J. Goyon, A. Colin, G. Ovarlez, A. Ajdari and L. Bocquet, *Nature*, 2008, **454**, 84–87.
24 N. Dubash and I. Frigaard, *J. Non-Newtonian Fluid Mech.*, 2007, **142**, 123–134.
25 F. G. Gandolfo and H. L. Rosano, *J. Colloid Interface Sci.*, 1997, **194**, 31–36.
26 A. Rust and M. Manga, *J. Non-Newtonian Fluid Mech.*, 2002, **104**, 53–63.
27 E. Llewellin, H. Mader and S. Wilson, *Proc. R. Soc. London, Ser. A*, 2002, **458**, 987–1016.
28 J. Palierne, *Rheol. Acta*, 1990, **29**, 204–214.
29 N.-T. Thuy Linh, L. Ducloué, G. Ovarlez and X. Chateau, *Poromechanics V: Proceedings of the Fifth Biot Conference on Poromechanics*, 2013, pp. 1895–1902.

